Original Article

The value of using a deep learning image reconstruction algorithm of thinner slice thickness to balance the image noise and spatial resolution in low-dose abdominal CT

Huan Wang[1#^], Xinyu Li[1#], Tianze Wang[2], Jianying Li[3], Tianze Sun[1], Lihong Chen[1], Yannan Cheng[1], Xiaoqian Jia[1], Xinyi Niu[1], Jianxin Guo[1]

[1]Department of Radiology, the First Affiliated Hospital of Xi'an Jiaotong University, Xi'an, China; [2]Department of Neurosurgery, Xi'an Jiaotong University School of Medicine, Xi'an, China; [3]GE Healthcare, Computed Tomography Research Center, Beijing, China

Contributions: (I) Conception and design: J Guo, H Wang; (II) Administrative support: J Guo; (III) Provision of study materials or patients: X Li, T Wang; (IV) Collection and assembly of data: T Sun, L Chen, Y Cheng, X Jia, X Niu; (V) Data analysis and interpretation: H Wang, J Li; (VI) Manuscript writing: All authors; (VII) Final approval of manuscript: All authors.

[#]These authors contributed equally to this work and should be considered as co-first authors.

Correspondence to: Dr. Jianxin Guo. Department of Radiology, the First Affiliated Hospital of Xi'an Jiaotong University, Xi'an, China. Email: gjx1665@xjtufh.edu.cn.

Background: Traditional reconstruction techniques have certain limitations in balancing image quality and reducing radiation dose. The deep learning image reconstruction (DLIR) algorithm opens the door to a new era of medical image reconstruction. The purpose of the study was to evaluate the DLIR images at 1.25 mm thickness in balancing image noise and spatial resolution in low-dose abdominal computed tomography (CT) in comparison with the conventional adaptive statistical iterative reconstruction-V at 40% strength (ASIR-V40%) at 5 and 1.25 mm.

Methods: This retrospective study included 89 patients who underwent low-dose abdominal CT. Five sets of images were generated using ASIR-V40% at a 5 mm slice thickness and 1.25 mm (high-resolution) with DLIR at 1.25 mm using 3 strengths: low (DLIR-L), medium (DLIR-M), and high (DLIR-H). Qualitative evaluation was performed for image noise, artifacts, and visualization of small structures, while quantitative evaluation was performed for standard deviation (SD), signal-to-noise ratio (SNR), and spatial resolution (defined as the edge rising slope).

Results: At 1.25 mm, DLIR-M and DLIR-H images had significantly lower noise (SD in fat: 14.29±3.37 and 9.65±3.44 HU, respectively), higher SNR for liver (3.70±0.78 and 5.64±1.20, respectively), and higher overall image quality (4.30±0.44 and 4.67±0.40, respectively) than did the respective values in ASIR-V40% images (20.60±4.04 HU, 2.60±0.63, and 3.77±0.43; all P values <0.05). Compared with the 5 mm ASIR-V40% images, the 1.25 mm DLIR-H images had lower noise (SD: 9.65±3.44 *vs.* 13.63±10.03 HU), higher SNR (5.64±1.20 *vs.* 4.69±1.28), and higher overall image quality scores (4.67±0.40 *vs.* 3.94±0.46) (all P values <0.001). In addition, DLIR-L, DLIR-M, and DLIR-H images had a significantly higher spatial resolution in terms of edge rising slope (59.66±21.46, 58.52±17.48, and 59.26±13.33, respectively, *vs.* 33.79±9.23) and significantly higher image quality scores in the visualization of fine structures (4.43±0.50, 4.41±0.49, and 4.38±0.49, respectively *vs.* 2.62±0.49) than did the 5 mm ASIR-V40 images.

Conclusions: The 1.25 mm DLIR-M and DLIR-H images had significantly reduced image noise and improved SNR and overall image quality compared to the 1.25 mm ASIR-V40% images, and they

^ ORCID: 0000-0001-5059-2962.

had significantly improved the spatial resolution and visualization of fine structures compared to the 5 mm ASIR-V40% images. DLIR-H images had further reduced image noise compared with the 5 mm ASIR-V40% images, and DLIR-H was the most effective technique at balancing the image noise and spatial resolution in low-dose abdominal CT.

Keywords: Deep learning; image reconstruction; different layer thickness; radiation dose

Submitted Apr 10, 2022. Accepted for publication Nov 03, 2022. Published online Nov 30, 2022.
doi: 10.21037/qims-22-353
View this article at: https://dx.doi.org/10.21037/qims-22-353

Introduction

The widespread use of computed tomography (CT) lies in its availability, speed, and diagnostic performance. Almost one-third of CT examinations involve the abdomen (1), and the related radiation exposure and potential carcinogenicity to this area has continued to attract research attention (2-4). Many of CT's benefits are overshadowed by concerns for persistent radiation dose, especially for young patients and patients undergoing repeated CT scans (2,5). Therefore, achieving dose reduction while maintaining image quality is an area of intense research focus.

Usually, we can achieve this objective by improving the technology of CT scanners and software (6). Traditional reconstruction methods, such as filtered back projection (FBP), generate higher image noise at reduced radiation doses, leading to image quality degradation. The improvement of computing power has given rise to iterative reconstruction (IR) technology. Many clinical studies have shown that these IR algorithms can be applied to reduce radiation dose (7-10). However, the nonlinear and nonstationary properties of IR algorithms cause the spatial resolution to become dependent on contrast and radiation dose. When applied at high levels, IR algorithms alter the texture of the images (11,12). The need to balance image noise and spatial resolution and image texture limits the ability of IR algorithms to further reduce the radiation dose.

Faced with these limitations of IR, GE Healthcare (Waukesha, WI, USA) developed deep learning image reconstruction (DLIR) algorithms (TrueFidelity) trained with high-quality FBP datasets of both patient and phantom scans to learn how to differentiate noise from signals. The design goal of the DLIR algorithm is to generate a reconstructed image that outperforms previous IR techniques in terms of image quality, dose performance, and reconstruction speed. The DLIR engine generates the output image from an input sonogram that is acquired with a low radiation dose using deep convolutional neural network (DCNN)-based models. During training, the DCNNs analyze the data and synthesize a reconstruction function, which is optimized through the learning process and extensive testing of the dataset for validation. The DLIR is an algorithm developed to achieve image qualities similar to those of high-dose FBP, as the FBP is the ideal image reconstruction technique in a high-dose and optimal-scan environment. The DLIR technique can be reconstructed in 3 modes: low (DLIR-L), medium (DLIR-M), and high (DLIR-H). The final output image is generated by varying the degree of the noise included in the image for each mode. The introduction of L, M, and H is intended to provide a good balance between noise reduction and improved spatial resolution, with L favoring spatial resolution and H favoring noise reduction. Therefore, our study aimed to evaluate the ability of the DLIR algorithm (TrueFidelity) in balancing image noise and spatial resolution in low-dose abdominal CT as compared with the conventional adaptive statistical iterative reconstruction-V (ASIR-V) algorithm.

Methods

Patient population

This retrospective study included 89 patients who underwent low-dose chest CT scans between May 2018 and August 2018. To ensure the complete inclusion of the entire chest, the scan range for the chest CT normally contains a small portion of the upper abdomen. The portion of the scan data for the upper abdomen included in the chest CT scan was used for the study. The image analysis for this paper was then limited to the anatomy and blood supplies of the upper abdomen. The study was conducted in accordance with the Declaration of Helsinki (as revised in 2013). The study was approved by the ethics board of the

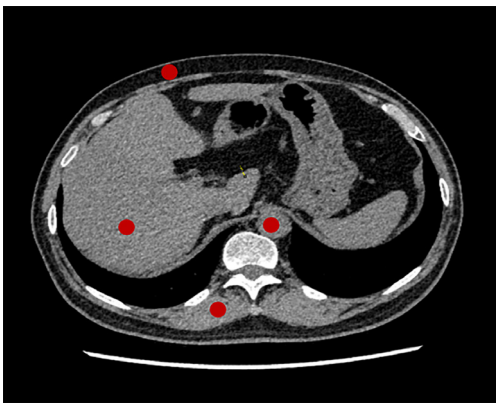

Figure 1 An example of image with four regions-of-interest placement for quantitative image measurement. The red dots indicate ROI in subcutaneous fat, liver parenchyma, paraspinal muscle and abdominal aorta was measured. ROI, region of interest.

First Affiliated Hospital of Xi'an Jiaotong University, and individual consent for this retrospective analysis was waived.

Data acquisition and image reconstruction

All patients underwent the low-dose chest CT scan on a 256-row multidetector CT system (Revolution CT, GE Healthcare). Patients were placed in the supine position, and scanning was performed in the craniocaudal direction in a single breath hold. The automatic tube current modulation technique (SmartmA) was used to automatically adjust the tube current for achieving consistent image quality across the study population. The scanning acquisition parameters were as follows: tube voltage, 120 kVp; tube current range, 10–130 mA; noise index value, 16; rotation time, 0.5 seconds; detector collimation, 128×0.625 mm; helical pitch, 0.992:1; and scan field of view, 50 cm with the "Largebody" bowtie filter. Using a high noise index value of 16 (than the normal 9 for the routine abdominal CT application) significantly reduced the required radiation dose.

The scan data for the upper abdomen were reconstructed into standard image set at 5 mm with ASIR-V at 40% (ASIR-V40%) blending percentage between FBP and ASIR-V for routine clinical use. Additionally, images at a thinner slice thickness of 1.25 mm were generated to simulate higher spatial resolution but lower-detected x-ray signal strength per detector cell using ASIR-V40% and DLIR at 3 reconstruction strength levels: DLIR-L, DLIR-M, and DLIR-H. All images were reconstructed using the "standard" reconstruction kernel, and image sets were transferred to workstations for data measurement and image analysis.

Quantitative analysis

Quantitative image analysis was performed on an Advantage Workstation (AW, Version 4.7, GE Healthcare) blindly by a radiologist who was board-certified in diagnostic radiology and had 5 years of experience in abdominal CT imaging. The CT attenuation value (CT value in HU) and standard deviation (SD) of abdominal subcutaneous fat, hepatic parenchyma, paraspinal muscle, and the abdominal aorta were measured using a region of interest (ROI) with a diameter of 5 mm on the image section containing the trunk of the portal vein. The copy-and-paste functions were used for ROI placement so that the same areas of interest could be drawn in the same location on each reconstruction. All measurements were performed 3 times over 3 consecutive slices under identical display window width (400 HU) and window level (40 HU) settings, with the average values being used for further analysis. ROIs were placed in a uniform area away from artifacts, as shown in *Figure 1*. Image quality is represented by image noise (SD) and signal-to-noise ratio (SNR; SNR = CT value/SD) (13,14).

To further quantitatively evaluate the spatial image resolution of different reconstruction algorithms, we also investigated the interface between fat and liver parenchyma. To do this, we used their contrast difference which has an adequate CT attenuation difference for measuring the spatial resolution by drawing a line from the fat to the liver parenchyma and measuring all CT values on the line, as shown in *Figures 2*,*3*. CT values of all the points on the line from fat to liver parenchyma were measured in ImageJ (S National Institutes of Health, Bethesda, MD, USA) by marking all the reconstructions in the same position. The CT value of the reconstructed image in the same position was imported into a Microsoft Excel table using ImageJ software. The data points between the last dip and the first peak on the profile curve were fitted using the slope formula to calculate the edge rising slope which was used to represent the spatial resolution of the image (*Figure 3*; *Table 1*).

Qualitative analysis

The qualitative images were assessed in terms of image noise, artifacts, and visualization of small structures by 2 blinded readers who were board-certified in diagnostic

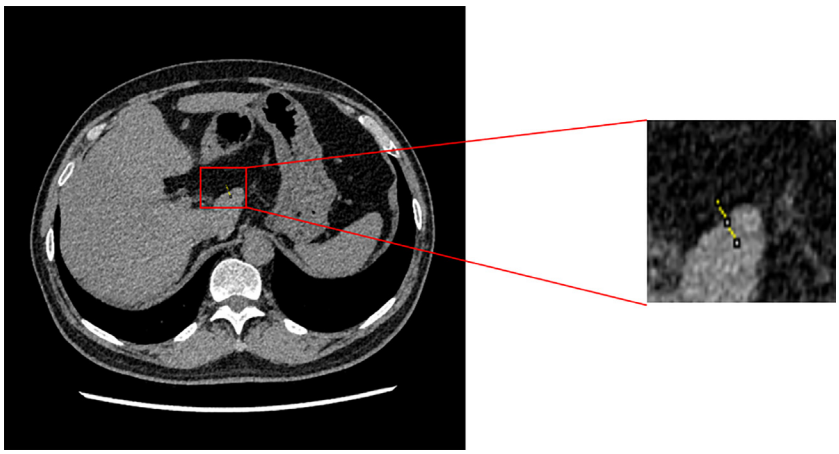

Figure 2 Schematic for measuring edge rising slope. The yellow lines in the right image indicate Ct values of all points from fat to liver parenchyma.

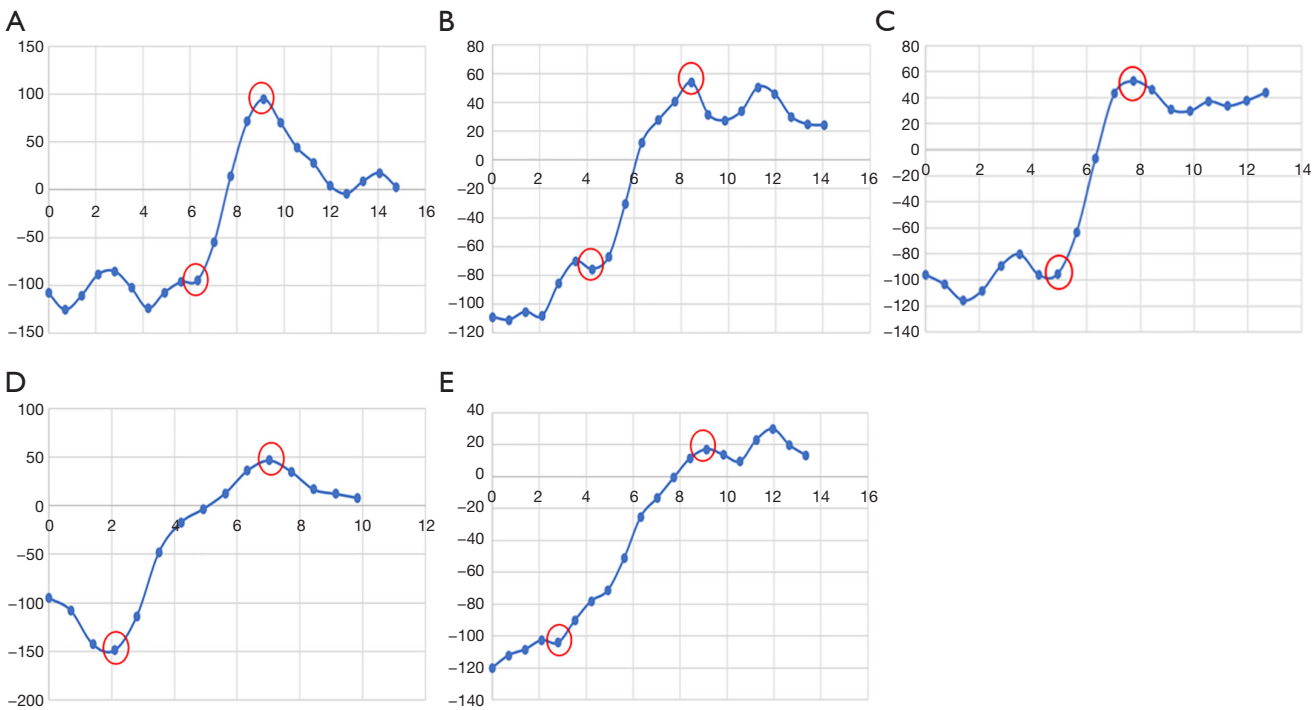

Figure 3 Profiles for measuring the edge rising slope between fat and liver parenchyma of a 61-year-old male. (A) 1.25 mm DLIR-L; (B) 1.25 mm DLIR-M; (C) 1.25 mm DLIR-H; (D) 1.25 mm ASIR-V40%; (E) 5 mm ASIR-V40%. The red circles indicate the data point between the last inclination and the first peak, the slope is used to represent the spatial resolution of the image. DLIR, deep learning image reconstruction; ASIR, adaptive statistical iterative reconstruction; 1.25 mm ASIR-V40%, 1.25 mm slice thickness images with ASIR-V40% algorithm; 5 mm ASIR-V40%, 5 mm slice thickness images with ASIR-V40% algorithm; L, low; M, medium; H high.

radiology and had at least 10 years of experience in abdominal CT imaging. The 2 radiologists were unaware of the examination details and examined each case independently after receiving standardized instructions. The reconstructed axial images with patient information deleted were displayed using a high-resolution monitor on a dual-monitor picture archiving and communication system (PACS) workstation (*Figure 4*; *Table 2*). The reader

Table 1 Spatial resolution comparison in terms of edge rising slope among the five different reconstructions

Group	1.25 mm ASIR-V40%	5 mm ASIR-V40%	1.25 mm DLIR-L	1.25 mm DLIR-M	1.25 mm DLIR-H	P1	P2	P3	P4	P5	P6	P7	P8	P9	P10
Edge rising slope	51.08±13.84	33.79±9.23	59.66±21.46	58.52±17.48	59.26±13.33	0.000	0.260	0.280	0.020	0.000	0.000	0.000	0.999	1.000	1.000

ASIR, adaptive statistical iterative reconstruction; DLIR, deep learning image reconstruction; 1.25 mm ASIR-V40%, 1.25 mm slice thickness images with ASIR-V40% algorithm; 5 mm ASIR-V40%, 5 mm slice thickness images with ASIR-V40% algorithm; L, low; M, medium; H high. P1, P value among the five groups; P2, P value between 1.25 mm ASiR40% and DLIR-L; P3, P value compared by the 1.25 ASIR *vs.* DLIR-M; P4:P value compared by the 1.25 mm ASIR *vs.* DLIR-H; P5, P value compared by the 5 mm ASIR *vs.* DLIR-L; P6, P value compared by the 5 mm ASIR *vs.* DLIR-M; P7, P value compared by the 5 mm ASIR *vs.* DLIR-H; P8, P value compared by the DLIR-L *vs.* DLIR-M; P9, P value of DLIR-L *vs.* DLIR-H group; P10, P value of DLIR-M *vs.* DLIR-H.

could adjust the image display window and level during the evaluation process. Qualitative image quality, including image noise, artifacts, edge sharpness of organs, and visualization of small structures (i.e., small blood vessels in the liver) was graded on a 5-point scale (15,16). *Table 3* lists the detailed evaluation criteria. Finally, the overall image quality was averaged over the scores of the 3 different categories to generate the final score, with a higher the score indicating a better image quality.

Statistical analysis

SPSS 25 software (IBM Corp., Armonk, NY, USA) was used to perform statistical analysis on the image quality of different reconstruction algorithms. Quantitative image measurements (CT value and SD) are expressed as mean ± SD ($\bar{x}$±s) and were compared with repeated-measures analysis of variance (ANOVA). Bonferroni correction or Games-Howell *post hoc* test was performed according to the homogeneity of variance. The qualitative image quality scores were compared using Friedman test, and Kappa statistics were used to test the consistency of the subjective image quality scores of the 2 radiologists. A kappa value between 0.81–1.00 was considered excellent, 0.61–0.80 acceptable, 0.41–0.60 medium, 0.21–0.40 general, and 0.00–0.20 poor. A P<0.05 indicated the difference is statistically significant (17).

Results

There were 83 males and 6 females in the study population, with an average age of 64±22 years (range, 49–86 years), an average body weight of 74.67±16.05 kg (range, 44–100 kg), and an average body mass index of 25.4±4.83 kg/m^2 (range, 16.54–35.43 kg/m^2). The volume CT dose index for the upper abdominal CT was 2.88±1.12 mGy. The CT dose index-volume (CTDIvol) values were calculated using the average tube currents for the upper abdominal portion of the scan, which were stored in the system during the chest-abdominal CT scan.

Quantitative image quality analysis

As shown in *Table 4* , there was no significant difference in CT value among the 5 different reconstruction groups. For the 1.25 mm slice thickness images, compared with ASIR-V40%, DLIR-M and DLIR-H decreased image noise by 30.6% and 53.2% in fat, 29.1% and 53.2% in the

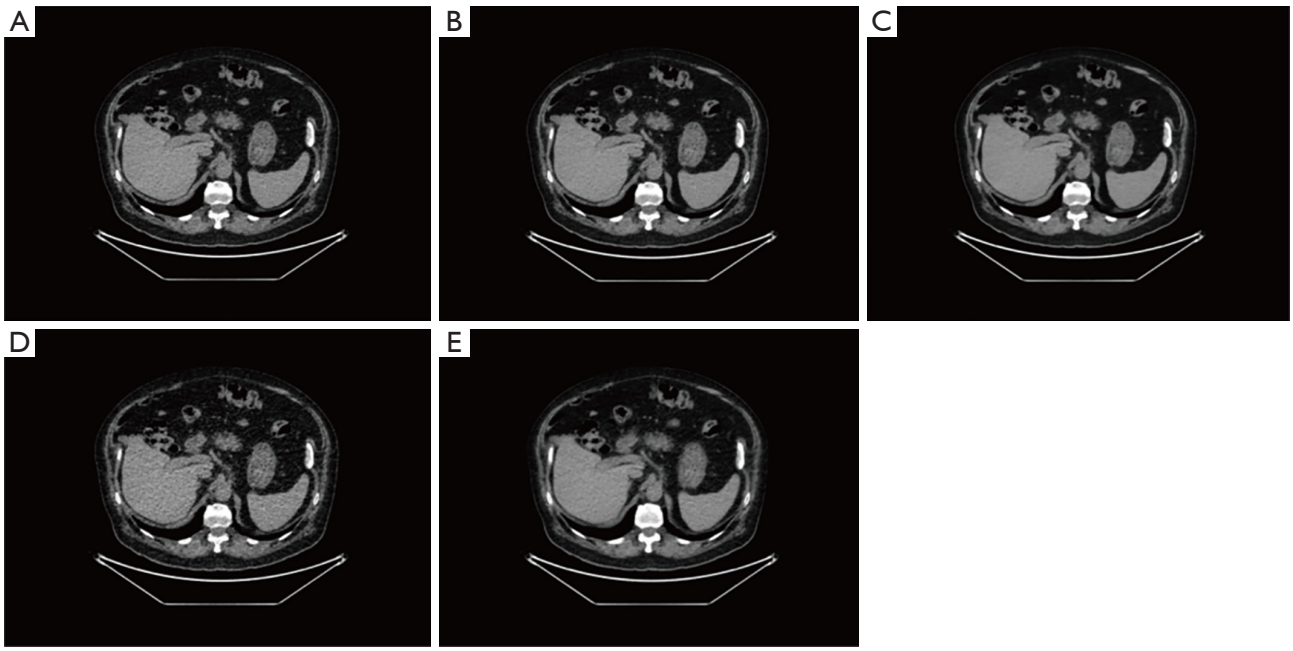

Figure 4 Comparison of CT images under different reconstruction algorithms. (A) 1.25 mm DLIR-L; (B) 1.25 mm DLIR-M; (C) 1.25 mm DLIR-H; (D) 1.25 mm ASIR-V40%; (E) 5 mm ASIR-V40%. CT, computed tomography; DLIR, deep learning image reconstruction; ASIR, adaptive statistical iterative reconstruction; 1.25 mm ASIR-V40%, 1.25 mm slice thickness images with ASIR-V40% algorithm; 5 mm ASIR-V40%, 5 mm slice thickness images with ASIR-V40% algorithm; L, low; M, medium; H high.

liver parenchyma, 28.8% and 52.4% in paraspinal muscle, and 27.3% and 51.3% in the abdominal aorta, respectively. Compared with the 5 mm slice thickness ASIR-V40%, the 1.25 mm DLIR-H reduced the image noise of fat by 29.2%, liver parenchyma by 16.7%, paraspinal muscle by 17.8%, and the abdominal aorta by 14.8%. In regard to SNR, the comparison was basically consistent with that of the noise.

As shown in *Table 1* and *Figure 2*, there was no significant statistical difference in the edge rising slope among the 3 DLIR groups. Compared with that of the 5 mm ASIR-V40% group, the edge rising slope of the DLIR-L, DLIR-M, and DLIR-H groups increased by 76.7%, 73.2%, and 75.4%, respectively. Compared that of the 1.25 mm ASIR-V40% group, the edge rising slope of the DLIR-H group increased by 16%.

Qualitative image quality analysis

As shown in *Table 2*, the consistency between the observations of the 2 readers was very good (kappa values ranged from 0.81 to 1.00). In terms of total image quality, the order of numerical scores from high to low was DLIR-H (1.25 mm) > DLIR-M (1.25 mm) > ASIR-V40% (5 mm) > DLIR-L (1.25 mm) > ASIR-V40% (1.25 mm). The order changed based on the individual evaluation criterion. In terms of image noise, the numerical scores from high to low were DLIR-H (1.25 mm) > ASIR-V40% (5 mm) > DLIR-M (1.25 mm) > DLIR-L (1.25 mm) > ASIR-V40% (1.25 mm). In terms of visualization of fine structures, the numerical scores from high to low were DLIR-L (1.25 mm) > DLIR-M (1.25 mm) > DLIR-H (1.25 mm) > ASIR-V40% (1.25 mm) > ASIR-V40% (5 mm). There was no statistically significant difference among the 3 DLIR groups, while the DLIR-L, DLIR-M, and DLIR-H groups had better image visualization than did the ASIR-V40% groups. Regarding image artifacts, there was no statistically significant difference between any of the groups.

Discussion

Our study compared the conventional ASIR-V40% images at the normal 5 mm slice thickness and the thin 1.25 mm thickness to the 3 strength levels of DLIR images at 1.25 mm slice thickness in low-dose abdominal CT. Our preliminary results showed that DLIR had strong advantages in balancing image noise and spatial resolution to provide

Table 2 Qualitative image quality comparison among five different reconstructions

Image assessment terms	1.25 mm ASIR-V40%	5 mm ASIR-V40%	DLIR-L	DLIR-M	DLIR-H	Kappa	P1	P2	P3	P4	P5	P6	P7	P8	P9	P10
Image noise	2.34±0.48	4.40±0.49	2.43±0.50	3.60±0.49	4.71±0.46	0.914	0.000	0.797	0.000	0.000	0.000	0.000	0.000	0.000	0.000	0.000
Visualization of small structures	4.19±0.40	2.62±0.49	4.43±0.50	4.41±0.49	4.38±0.49	0.885	0.000	0.008	0.019	0.058	0.000	0.000	0.000	1.000	0.980	0.999
Image artifacts	4.79±0.42	4.80±0.40	4.84±0.37	4.88±0.33	4.93±0.27	0.902	0.047	0.949	0.543	0.750	0.991	0.733	0.152	0.968	0.428	0.875
Total image quality scores	3.77±0.43	3.94±0.46	3.90±0.46	4.30±0.44	4.67±0.40	–	0.000	0.005	0.000	0.000	0.822	0.000	0.000	0.000	0.000	0.000

ASIR, adaptive statistical iterative reconstruction; DLIR, deep learning image reconstruction; 1.25 mm ASIR-V40%, 1.25 mm slice thickness images with ASIR-V40% algorithm; 5 mm ASIR-V40%, 5 mm slice thickness images with ASIR-V40% algorithm. P1, P value among the five groups, P2, P value between 1.25 mm ASIR40% and DLIR-L, P3, P value compared by the 1.25 ASIR *vs.* DLIR-M, P4:P value compared by the 1.25 mm ASIR *vs.* DLIR-H, P5, P value compared by the 5 mm ASIR *vs.* DLIR-L, P6, P value compared by the 5 mm ASIR *vs.* DLIR-M, P7, P value compared by the 5 mm ASIR *vs.* DLIR-H, P8, P value compared by the DLIR-L *vs.* DLIR-M. P9, P value of DLIR-L *vs.* DLIR-H group, P10, P value of DLIR-M *vs.* DLIR-H.

better overall image quality under low-dose conditions. Compared with the standard ASIR-V40%, DLIR-M and DLIR-H significantly improved the quantitative and qualitative image quality of abdominal sections under the same thin image slice thickness of 1.25 mm. Compared with the commonly used ASIR-V40% at 5 mm, the 1.25 mm DLIR-H, at a quarter of the signal strength, still provided lower noise images at significantly improved spatial resolution.

Conventionally, there is an inverse relationship between image noise and spatial resolution, which has been noted as one of the limitations of many IR algorithms. The ASIR-V algorithm has the advantage of reducing noise (18), but it is difficult to balance image noise and spatial resolution when high-strength ASIR-V is used (15). Studies have confirmed the limitations of texture alteration in high-strength ASIR-V images and have shown that excessively lower radiation dose levels increase the risk of an inaccurate diagnosis, such as in the detection of liver lesions (16,17). One study has indicated that although the use of 80% of ASIR-V significantly reduced noise and improved CNR, the images were so smooth that they had a negative impact on the diagnosis of lesions (19). On the other hand, DLIR is designed to maintain texture and spatial resolution while reducing noise, so it is expected to significantly impact the optimization of the abdominal CT scheme. Clinical studies have demonstrated that deep learning-based image reconstruction methods have higher diagnostic accuracy compared to IR algorithms (20,21). Phantom studies have shown that DLIR improves the image quality of CT scans at medium or lower radiation doses (22). Benz *et al.* (23) found that, compared with ASIR-V, DLIR significantly reduces noise while providing excellent image quality and the same diagnostic accuracy. Akagi *et al.* (24) found that DLIR-H could clearly show small metastases on low-dose scans. Higaki *et al.* (22) conducted a prospective study of 59 patients who underwent standard-dose chest or abdominal pelvic CT and found that all pulmonary nodules detected at the standard dose were also detected by DLIR at a low dose. Sun *et al.* (25,26) found that the DLIR algorithm could also significantly reduce the contrast agent dose and radiation dose in angiography. The results of our current research showed that DLIR could reduce image noise and significantly improve objective and subjective image quality without excessive smoothing. DLIR-H reduced image noise by more than 50% compared with ASIR-V40% for the 1.25 mm slice thickness images while showing better boundaries with a higher edge rise slope (P=0.02) and

Table 3 Criteria for image quality evaluation

Score	Noise	Artifacts	Edge sharpness and visualization of small structures
5	Minimal image noise	No artifacts	Very clear margins and excellent visualization of small structures
4	Less than average noise	Minor artifacts not interfering with diagnostic decision making	Clear margins and good visualization of small structures
3	Average image noise	Some artifacts affecting visualization of small structures, diagnosis still possible	Slightly blurred margins but small structures still recognizable
2	Above average noise	Major artifacts affecting visualization of major structures, diagnosis not certain	blurred margins and uncertain in visualization of small structures
1	Unacceptable image noise	Severe artifacts affecting diagnosis	Unable to define object and margins

Table 4 Comparison of the quantitative measurements among the five different reconstructions

Tissue	1.25 mm ASIR-V40%	5 mm ASIR-V40%	1.25 mm DLIR-L	1.25 mm DLIR-M	1.25 mm DLIR-H	P1	P2	P3	P4	P5	P6	P7	P8	P9	P10
Fat AV	−103.01±13.98	−102.46±13.93	−102.55±12.72	−102.31±12.54	−102.17±12.41	0.999	1.000	1.000	1.000	1.000	1.000	1.000	1.000	1.000	1.000
Liver AV	57.28±10.50	57.29±9.37	57.95±9.62	57.95±9.12	58.03±8.69	0.986	1.000	1.000	1.000	1.000	1.000	1.000	1.000	1.000	1.000
Muscle AV	52.16±8.31	51.99±6.51	52.68±7.16	52.63±6.44	52.59±5.80	0.916	1.000	1.000	1.000	1.000	1.000	1.000	1.000	1.000	1.000
Aorta AV	45.79±8.85	46.13±6.18	46.69±6.69	46.39±6.16	46.77±4.94	0.804	1.000	1.000	1.000	1.000	1.000	1.000	1.000	1.000	1.000
Fat SD	20.60±4.04	13.63±10.03	18.78±3.61	14.29±3.37	9.65±3.44	0.000	0.364	0.000	0.000	0.000	1.000	0.000	0.000	0.000	0.000
Liver SD	22.56±3.27	12.69±2.37	21.15±2.75	15.99±2.19	10.56±1.79	0.000	0.032	0.000	0.000	0.000	0.000	0.000	0.000	0.000	0.000
Muscle SD	23.27±3.40	13.47±3.02	21.85±3.17	16.57±2.59	11.07±2.08	0.000	0.560	0.000	0.000	0.000	0.000	0.000	0.000	0.000	0.000
Aorta SD	25.84±3.52	14.76±2.57	24.59±3.25	18.79±2.74	12.58±2.38	0.000	0.156	0.000	0.000	0.000	0.000	0.000	0.000	0.000	0.000
Fat SNR	−5.24±1.41	−8.72±2.84	−5.7±1.42	−7.59±2.06	−11.7±3.66	0.000	0.271	0.000	0.000	0.000	0.038	0.000	0.000	0.000	0.000
Liver SNR	2.60±0.63	4.69±1.28	2.79±0.61	3.70±0.78	5.64±1.20	0.000	0.339	0.000	0.000	0.000	0.000	0.000	0.000	0.000	0.000
Muscle SNR	2.29±0.50	4.07±1.11	2.46±0.47	3.25±0.62	4.92±1.03	0.000	0.224	0.000	0.000	0.000	0.000	0.000	0.000	0.000	0.000
Aorta SNR	1.80±0.42	3.22±0.69	1.93±0.38	2.52±0.52	3.86±0.88	0.000	0.294	0.000	0.000	0.000	0.000	0.000	0.000	0.000	0.000

AV, attenuation value; SD, standard deviation; SNR, signal-to-noise ratio; ASIR, adaptive statistical iterative reconstruction; DLIR, deep learning image reconstruction; 1.25 mm ASIR-V40%, 1.25 mm slice thickness images with ASIR-V40% algorithm; 5 mm ASIR-V40%, 5 mm slice thickness images with ASIR-V40% algorithm; L, low; M, medium; H high. P1, P value among the five groups; P2, P value between 1.25 mm ASIR40% and DLIR-L; P3, P value compared by the 1.25ASIR *vs.* DLIR-M; P4: P value compared by the 1.25 mm ASIR *vs.* DLIR-H; P5, P value compared by the 5 mm ASIR *vs.* DLIR-L; P6, P value compared by the 5 mm ASIR *vs.* DLIR-M; P7, P value compared by the 5 mm ASIR *vs.* DLIR-H; P8, P value compared by the DLIR-L *vs.* DLIR-M; P9, P value of DLIR-L *vs.* DLIR-H group; P10, P value of DLIR-M *vs.* DLIR-H.

close to statistically significant higher subjective score in the visualization of small structures (P=0.058). DLIR-H also demonstrated its strong ability to balance high spatial resolution and low image noise. Liver CT has a stringent requirement for high low-contrast resolution. Traditionally, thick slice thickness images (i.e., 5 mm) have been used in liver CT to achieve low noise images without requiring an excessive radiation dose in patients. With DLIR, this balanced requirement could be easily achieved. In fact, our results indicated that DLIR-H generated lower noise images at 1.25 mm slice thickness than did ASIR-V40% at 5 mm slice thickness, with significantly improved spatial image resolution in terms of the quantitative measurement of edge rising slope and the qualitative score of visualization of small structures (both P values <0.001). Furthermore, we believe that the DLIR algorithm may also be used on the datasets of the newly introduced photon-counting detector CT (27), which might improve image quality even more. This would enable scanning at lower doses and may even be applicable to a wide variety of pathologies.

This study has some limitations. First, we mainly focused on the subjective and objective evaluation of image quality but did not evaluate the impact of DLIR on the detection and diagnosis of specific lesions. A dedicated liver CT with contrast enhancement is needed for such an evaluation. Second, this study was limited by the small sample size. Further studies with larger sample sizes are needed to further validate our results.

In summary, our study indicates that DLIR, especially the highest strength DLIR, has a significantly higher ability to reduce image noise and balance image noise, noise texture, and spatial resolution than does the conventional ASIR-V algorithm. It is possible for DLIR to significantly reduce the radiation dose while preserving the exploratory and diagnostic capability of abdominal CT.

Acknowledgments

Funding: This work was supported by the Institutional Foundation of The First Affiliated Hospital of Xi'an Jiaotong University (No. 2021ZXY-04).

Footnote

Conflicts of Interest: All authors have completed the ICMJE uniform disclosure form (available at https://qims.amegroups.com/article/view/10.21037/qims-22-353/coif). JL is an employee of GE Healthcare. The article does not conflict with the company's declaration of interest. The other authors have no conflicts of interest to declare.

Ethical Statement: The authors are accountable for all aspects of the work in ensuring that questions related to the accuracy or integrity of any part of the work are appropriately investigated and resolved. The study was conducted in accordance with the Declaration of Helsinki (as revised in 2013). The study was approved by the ethics board of the First Affiliated Hospital of Xi'an Jiaotong University, and individual consent for this retrospective analysis was waived.

References

1. Stoker J, van Randen A, Laméris W, Boermeester MA. Imaging patients with acute abdominal pain. Radiology 2009;253:31-46.
2. Coakley FV, Gould R, Yeh BM, Arenson RL. CT radiation dose: what can you do right now in your practice? AJR Am J Roentgenol 2011;196:619-25.
3. Levin DC, Rao VM, Parker L. The recent downturn in utilization of CT: the start of a new trend? J Am Coll Radiol 2012;9:795-8.
4. Moreno CC, Hemingway J, Johnson AC, Hughes DR, Mittal PK, Duszak R Jr. Changing Abdominal Imaging Utilization Patterns: Perspectives From Medicare Beneficiaries Over Two Decades. J Am Coll Radiol 2016;13:894-903.
5. Hong JY, Han K, Jung JH, Kim JS. Association of Exposure to Diagnostic Low-Dose Ionizing Radiation With Risk of Cancer Among Youths in South Korea. JAMA Netw Open 2019;2:e1910584.
6. Sagara Y, Hara AK, Pavlicek W, Silva AC, Paden RG, Wu Q. Abdominal CT: comparison of low-dose CT with adaptive statistical iterative reconstruction and routine-dose CT with filtered back projection in 53 patients. AJR Am J Roentgenol 2010;195:713-9.

7. Katsura M, Matsuda I, Akahane M, Sato J, Akai H, Yasaka K, Kunimatsu A, Ohtomo K. Model-based iterative reconstruction technique for radiation dose reduction in chest CT: comparison with the adaptive statistical iterative reconstruction technique. Eur Radiol 2012;22:1613-23.
8. Larbi A, Orliac C, Frandon J, Pereira F, Ruyer A, Goupil J, Macri F, Beregi JP, Greffier J. Detection and characterization of focal liver lesions with ultra-low dose computed tomography in neoplastic patients. Diagn Interv Imaging 2018;99:311-20.
9. Macri F, Greffier J, Khasanova E, Claret PG, Bastide S, Larbi A, Bobbia X, Pereira FR, de la Coussaye JE, Beregi JP. Minor Blunt Thoracic Trauma in the Emergency Department: Sensitivity and Specificity of Chest Ultralow-Dose Computed Tomography Compared With Conventional Radiography. Ann Emerg Med 2019;73:665-70.
10. Kim HG, Lee HJ, Lee SK, Kim HJ, Kim MJ. Head CT: Image quality improvement with ASIR-V using a reduced radiation dose protocol for children. Eur Radiol 2017;27:3609-17.
11. Verdun FR, Racine D, Ott JG, Tapiovaara MJ, Toroi P, Bochud FO, Veldkamp WJH, Schegerer A, Bouwman RW, Giron IH, Marshall NW, Edyvean S. Image quality in CT: From physical measurements to model observers. Phys Med 2015;31:823-43.
12. Samei E, Richard S. Assessment of the dose reduction potential of a model-based iterative reconstruction algorithm using a task-based performance metrology. Med Phys 2015;42:314-23.
13. Parakh A, Cao J, Pierce TT, Blake MA, Savage CA, Kambadakone AR. Sinogram-based deep learning image reconstruction technique in abdominal CT: image quality considerations. Eur Radiol 2021;31:8342-53.
14. Jensen CT, Liu X, Tamm EP, Chandler AG, Sun J, Morani AC, Javadi S, Wagner-Bartak NA. Image Quality Assessment of Abdominal CT by Use of New Deep Learning Image Reconstruction: Initial Experience. AJR Am J Roentgenol 2020;215:50-7.
15. Gatti M, Marchisio F, Fronda M, Rampado O, Faletti R, Bergamasco L, Ropolo R, Fonio P. Adaptive Statistical Iterative Reconstruction-V Versus Adaptive Statistical Iterative Reconstruction: Impact on Dose Reduction and Image Quality in Body Computed Tomography. J Comput Assist Tomogr 2018;42:191-6.
16. McCollough CH, Yu L, Kofler JM, Leng S, Zhang Y, Li Z, Carter RE. Degradation of CT Low-Contrast Spatial Resolution Due to the Use of Iterative Reconstruction and Reduced Dose Levels. Radiology 2015;276:499-506.
17. Jensen CT, Wagner-Bartak NA, Vu LN, Liu X, Raval B, Martinez D, Wei W, Cheng Y, Samei E, Gupta S. Detection of Colorectal Hepatic Metastases Is Superior at Standard Radiation Dose CT versus Reduced Dose CT. Radiology 2019;290:400-9.
18. Cao L, Liu X, Li J, Qu T, Chen L, Cheng Y, Hu J, Sun J, Guo J. A study of using a deep learning image reconstruction to improve the image quality of extremely low-dose contrast-enhanced abdominal CT for patients with hepatic lesions. Br J Radiol 2021;94:20201086.
19. Li LL, Wang H, Song J, Shang J, Zhao XY, Liu B. A feasibility study of realizing low-dose abdominal CT using deep learning image reconstruction algorithm. J Xray Sci Technol 2021;29:361-72.
20. Hong JH, Park EA, Lee W, Ahn C, Kim JH. Incremental Image Noise Reduction in Coronary CT Angiography Using a Deep Learning-Based Technique with Iterative Reconstruction. Korean J Radiol 2020;21:1165-77.
21. Narita K, Nakamura Y, Higaki T, Akagi M, Honda Y, Awai K. Deep learning reconstruction of drip-infusion cholangiography acquired with ultra-high-resolution computed tomography. Abdom Radiol (NY) 2020;45:2698-704.
22. Higaki T, Nakamura Y, Zhou J, Yu Z, Nemoto T, Tatsugami F, Awai K. Deep Learning Reconstruction at CT: Phantom Study of the Image Characteristics. Acad Radiol 2020;27:82-7.
23. Benz DC, Benetos G, Rampidis G, von Felten E, Bakula A, Sustar A, Kudura K, Messerli M, Fuchs TA, Gebhard C, Pazhenkottil AP, Kaufmann PA, Buechel RR. Validation of deep-learning image reconstruction for coronary computed tomography angiography: Impact on noise, image quality and diagnostic accuracy. J Cardiovasc Comput Tomogr 2020;14:444-51.
24. Akagi M, Nakamura Y, Higaki T, Narita K, Honda Y, Zhou J, Yu Z, Akino N, Awai K. Deep learning reconstruction improves image quality of abdominal ultra-high-resolution CT. Eur Radiol 2019;29:6163-71.
25. Sun J, Li H, Li J, Cao Y, Zhou Z, Li M, Peng Y. Performance evaluation of using shorter contrast injection and 70 kVp with deep learning image reconstruction for reduced contrast medium dose and radiation dose in coronary CT angiography for children: a pilot study. Quant Imaging Med Surg 2021;11:4162-71.
26. Sun J, Li H, Li J, Yu T, Li M, Zhou Z, Peng Y. Improving the image quality of pediatric chest CT angiography with low radiation dose and contrast volume using deep

learning image reconstruction. Quant Imaging Med Surg 2021;11:3051-8.
27. Decker JA, Bette S, Lubina N, Rippel K, Braun F, Risch F, Woźnicki P, Wollny C, Scheurig-Muenkler C, Kroencke TJ, Schwarz F. Low-dose CT of the abdomen: Initial experience on a novel photon-counting detector CT and comparison with energy-integrating detector CT. Eur J Radiol 2022;148:110181.

Cite this article as: Wang H, Li X, Wang T, Li J, Sun T, Chen L, Cheng Y, Jia X, Niu X, Guo J. The value of using a deep learning image reconstruction algorithm of thinner slice thickness to balance the image noise and spatial resolution in low-dose abdominal CT. Quant Imaging Med Surg 2023;13(3):1814-1824. doi: 10.21037/qims-22-353

